Ionic diffusion within the α^* and β phases of Ag_3SI

2007 J. Phys.: Condens. Matter 19 406214

(http://iopscience.iop.org/0953-8984/19/40/406214)

IOP PUBLISHING JOURNAL OF PHYSICS: CONDENSED MATTER

J. Phys.: Condens. Matter **19** (2007) 406214 (16pp) doi:10.1088/0953-8984/19/40/406214

Ionic diffusion within the α^* and β phases of Ag_3SI

S Hull[1,5], D A Keen[1,2], P A Madden[3] and M Wilson[4]

[1] The ISIS Facility, Rutherford Appleton Laboratory, Chilton, Didcot, Oxon OX11 0QX, UK
[2] Physics Department, Oxford University, Parks Road, Oxford OX1 3PU, UK
[3] Chemistry Department, Edinburgh University, The Kings Building, West Mains Road, Edinburgh EH9 3JJ, UK
[4] Department of Chemistry, University College London, Christopher Ingold Laboratories, 20 Gordon Street, London WC1H 0AJ, UK

E-mail: s.hull@rl.ac.uk

Received 21 June 2007
Published 12 September 2007
Online at stacks.iop.org/JPhysCM/19/406214

Abstract

The ionic diffusion mechanism of mobile ions within an underlying body-centred cubic (bcc) sublattice of immobile counterions is discussed. In particular, the case of equal numbers of two ionic species forming long-range ordered and disordered bcc arrays is considered, since these form the basis of the cubic perovskite and α-AgI-type crystal structures, respectively. Their structural behaviour, and its influence on the dynamic ionic disorder which characterizes superionic conduction, is illustrated for the case of Ag^+ diffusion within the β and α^* phases of Ag_3SI. The calculated behaviour obtained by molecular dynamics (MD) computer simulations is validated with reference to published neutron diffraction and ionic conductivity measurements of Ag_3SI, and used to examine the preferred diffusion pathways. The relevance of these findings for the anion conduction mechanisms within perovskite structured compounds is briefly discussed.

(Some figures in this article are in colour only in the electronic version)

1. Introduction

Superionics are compounds which display exceptionally high ('liquid-like') values of their ionic conductivity, σ, whilst in the solid state [1, 2]. Silver iodide, AgI, is commonly chosen as the 'textbook' example to illustrate superionic behaviour, since it undergoes a first-order structural phase transition at 420 K characterized by an abrupt increase in σ of over three orders of magnitude (for a review devoted to AgI, see [3]). Within the high-temperature α phase of AgI the ionic conductivity has a value $\sim 1\ \Omega^{-1}\ cm^{-1}$, increasing only slightly with temperature and actually falling by around 12% at the melting temperature of 829 K [4]. The crystal structure

[5] Author to whom any correspondence should be addressed.

of α-AgI comprises an immobile body-centred cubic (bcc) array of I^-, which contains a large number of octahedrally (*oct*) and tetrahedrally (*tet*) coordinated interstices [5]. The Ag^+ have been shown to undergo rapid jump diffusion, predominantly between the nearest-neighbour tet cavities in ⟨110⟩ directions rather than via the *oct* sites in ⟨100⟩ directions [6].

α-AgI is one member of a family of binary and ternary superionic phases with highly mobile Ag^+ or Cu^+ ions, some of which are alternatively characterized by face-centred cubic (fcc) or hexagonal close-packed (hcp) anion sublattices (see [2] and references therein). Those adopting the bcc arrangement might be expected to possess higher values of σ because the number of available interstices is higher in a bcc array (6 × tet and 3 × oct per immobile ion) than fcc or hcp ones (2 × tet and 1 × oct per immobile ion in both cases) [2, 7]. This suggestion is supported by experimental observations of the comparative ionic conductivities within the binary CuX (X = Br and I) halides [8], the binary Ag_2X (X = S and Te) chalcogenides [9] and Ag^+-rich ternary phases within the AgI–MI_2 (M = Cd, Hg, Pb, Sn and Zn) systems [10–13].

The principal aim of this study is to examine the role of a bcc structured immobile sublattice formed by two different ionic species in promoting (or hindering) extensive disorder of the counterions. In particular, the crystallographic consequences of the long-range ordering of equal numbers of *A* and *B* ions within a bcc structured sublattice will be considered, illustrated by the specific system Ag_3SI. This compound is the only ternary compound within the AgI–Ag_2S phase diagram [14] and it has been the subject of detailed experimental investigations using neutron diffraction and impedance spectroscopy techniques [15–17]. At temperatures above ≈520 K, Ag_3SI exists as the superionic α phase ($\sigma \sim 1.5\ \Omega^{-1}\ cm^{-1}$) in which the S^{2-} and I^- are randomly distributed over the sites of the bcc anion sublattice [15]. This high-temperature phase can be retained at room temperature by rapid quenching, with the resultant material (labelled α^*-Ag_3SI) possessing the disordered $S^{2-} + I^-$ sublattice and displaying a high ionic conductivity ($\sigma \sim 1.3 \times 10^{-1}\ \Omega^{-1}\ cm^{-1}$ at around 300 K). By contrast, slow cooling from the α phase followed by prolonged annealing at temperatures in the region of 450 K promotes ordering of the two anion species, forming the β phase, which has an ionic conductivity around two orders of magnitude lower than α^*-Ag_3SI (see figure 1) [17, 18]. On further cooling, the β phase transforms to the rhombohedral γ phase (space group $R3$ [15]) at ∼157 K, but no low-temperature transitions are observed in the case of α^*-Ag_3SI [18].

Clearly, it is important to understand the origin of the significantly higher ionic conductivity within the anion-disordered α^* phase compared to its anion-ordered β phase counterpart, both to clarify the fundamental structure–property relationships within this compound and, more widely, to inform the quest for improved ionically conducting materials to meet technological applications in, for example, lightweight solid-state batteries, high-capacity fuel cells and fast-response gas sensors. However, before addressing these issues, it is instructive to summarize the crystallographic description of the bcc sublattice and the various interstices formed within it.

2. Crystallographic considerations

A bcc sublattice formed by immobile ions of a single type *A* is illustrated in figure 2(a). There are two *A* ions within the unit cell which occupy the 2*a* positions of space group $Im\bar{3}m$ at 0, 0, 0 and $\frac{1}{2}, \frac{1}{2}, \frac{1}{2}$. The centres of the octahedral (*oct*) and tetrahedral (*tet*) cavities are described by the 6*b* sites at 0, $\frac{1}{2}, \frac{1}{2}$, etc, and the 12*d* sites at $\frac{1}{4}$, 0, $\frac{1}{2}$, etc, respectively. However, both these cavities are rather distorted. The octahedral environment of *A* ions around the *oct* positions contains the 'correct' *A*–*oct*–*A* angles (twelve with 90° and three with 180°) but the *oct*–*A* distances comprise four at $a/\sqrt{2}$ (where *a* is the cubic lattice parameter) plus two shorter

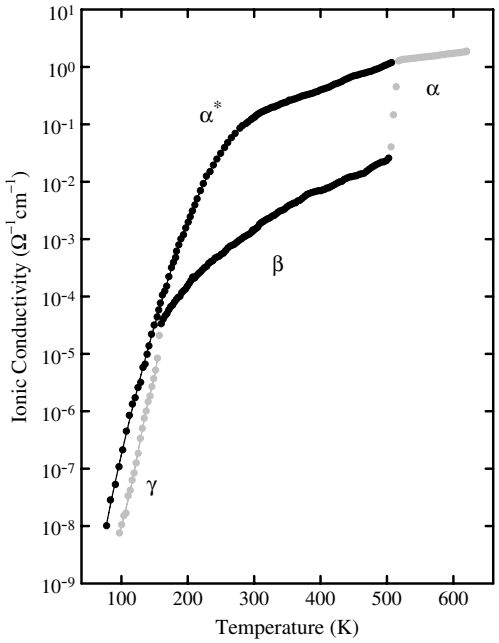

Figure 1. The temperature dependence of the ionic conductivity of Ag_3SI. At temperatures close to ambient the anion-disordered α^* phase (formed by quenching from the α phase) possesses an ionic conductivity around two orders of magnitude higher than the anion-ordered β phase (formed by prolonged annealing at around 450 K) [17]. The ionic conductivities of the high-temperature α and low-temperature γ phases are shown for comparison, but not considered in the course of this work.

contacts at distances of $a/2$. By contrast, the *tet–A* contacts are all equal, with four distances of $\sqrt{5}a/4$, but the *A–tet–A* angles comprise four with $2\sin^{-1}\sqrt{3/5} = 101.5°$ and two with $2\sin^{-1}\sqrt{4/5} = 126.9°$, which span the 'ideal' arrangement of six with $2\sin^{-1}\sqrt{2/3} = 109.5°$. This has important consequences when the bcc sublattice is comprised of two different species, *A* and *B*.

If the *A* and *B* species are randomly distributed over the 0, 0, 0 and $\frac{1}{2}, \frac{1}{2}, \frac{1}{2}$ positions within the cubic unit cell then a Bragg diffraction experiment, which measures the contents of the unit cell averaged over all unit cells and over time, can be modelled using identical 'average' ions on the 2*a* sites of space group $Im\bar{3}m$. This is referred to as an 'α-AgI' structure[6]. However, if the *A* and *B* species are ordered over the 0, 0, 0 and $\frac{1}{2}, \frac{1}{2}, \frac{1}{2}$ positions, respectively[7], the symmetry is lowered to $Pm\bar{3}m$ and (assuming that the two species have different scattering powers) Bragg peaks will be observed with *hkl* indices which violate the $h + k + l = 2n$ condition imposed by the presence of the body-centre translation symmetry operation.

The lowering of symmetry from $Im\bar{3}m$ to $Pm\bar{3}m$ causes the 6*b* set of *oct* positions within the former to be split into two symmetry-independent sets of three in 3*d* at $\frac{1}{2}$, 0, 0, etc, and 3*c* at 0, $\frac{1}{2}$, $\frac{1}{2}$, etc. The differences between the two sets are illustrated in figure 2(b). The 3*d* sites,

[6] Compounds with *A* and *B* as anions and *X* as cations are described as 'α-AgI' structured, whilst those with two species of cations on the *A* and *B* sites and *X* anions are called 'anti-α-AgI' structured.

[7] The assignment of labels of the two species to the two sites is, of course, arbitrary. However, this choice is made to be consistent with the conventional description of ABX_3 compounds with the perovskite structure which is introduced later.

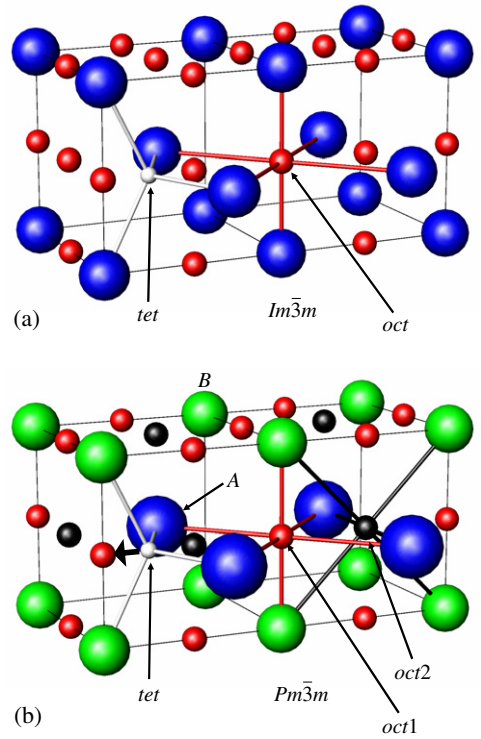

Figure 2. Schematic diagram illustrating (a) the locations of the octahedrally (*oct*) and tetrahedrally (*tet*) coordinated interstices within a bcc structured sublattice formed by a single ionic species. The outlines of two cubic unit cells are shown and, for clarity, only a single *tet* site is illustrated. In (b) the bcc sublattice is formed by an ordered array of A and B cations. The lowering of symmetry from $Im\bar{3}m$ to $Pm\bar{3}m$ generates two inequivalent subsets of octahedral cavities, with the *oct*1 sites favoured over the *oct*2 ones if $R_A > R_B$ (see text).

which we label *oct*1, have two B cations at the shorter distance of $a/2$ and four A cations at $a/\sqrt{2}$. In contrast, the 3*c* positions (*oct*2) have two A ions as their shorter contacts and four B cations at the longer distance. This distinction becomes important if the A ions are (arbitrarily) chosen to be larger than the B ions. Since the *oct*1 sites have the smaller counterions at the shorter distance they are likely to be energetically favoured over the *oct*2 positions, which have the larger species at $a/2$. If all the *oct*1 sites were filled with X counterions the stoichiometry would be ABX_3 and the ionic distribution would more conventionally be described as a cubic perovskite structure[8]. The tetrahedral interstices remain in a single 12-fold set during the reduction in symmetry from $Im\bar{3}m$ to $Pm\bar{3}m$, forming the 12*h* sites at x, 0, $\frac{1}{2}$, etc. However, as illustrated by the arrow in figure 2(b), the effect of the larger A species is to 'push' the favoured positions of the *tet* interstices from $x = \frac{1}{4}$ towards the *oct*1 sites at $x = 0$.

The discussion given above suggests that, for a hypothetical superionic conductor and on purely steric grounds, the transformation of the immobile sublattice from a monatomic bcc array (space group $Im\bar{3}m$) to an ordered array of two species of different sizes (space group $Pm\bar{3}m$) changes the lattice from one containing numerous available interstices (twelve *tet* plus six *oct*) into one containing only three (larger) cavities centred around the *oct*1 positions.

[8] Compounds with A and B as cations and X as anions are described as perovskite structured, whilst those with two species of anions on the A and B sites and X cations are called anti-perovskite structured.

Table 1. Summary of the parameters adopted in the interionic potentials used to perform molecular dynamics simulations of Ag_3SI, and based on those published previously for AgI [21] and Ag_2S [28, 29]. For comparison, the values used previously for MD studies of solid and molten Ag_3SI [19, 20] are included (in brackets) in those cases where they differ from those used in this work. The A_{ij} describe the short-range repulsive strength for ions i and j and W_{ij} are the coefficients of the van der Waals interaction. The R_i, Z_i and α_i denote the ionic radius, ionic charge and electronic polarizabilities of ion i, respectively.

Ionic species i and j	A_{ij}	W_{ij}
Ag^+–Ag^+	0.013 70 (0.0123)	0
Ag^+–S^{2-}	0.015 02 (0.0150)	0
Ag^+–I^-	0.012 37 (0.0123)	0
S^{2-}–S^{2-}	0.015 02 (0.0150)	0
S^{2-}–I^-	0.013 70 (0.0123)	3.47 (0)
I^-–I^-	0.012 37 (0.0123)	6.93 (0)

Ionic species i	R_i (Å)	Z_i	α_i (Å^2)
Ag^+	0.62 (0.69)	+0.60	0
S^{2-}	2.10 (2.11)	−1.20	6.52
I^-	2.83 (2.11)	−0.60	6.52

Intuitively, one would then expect that compounds formed by an ordered (perovskite-like) array of A and B species would have lower ionic conductivities than those with disordered (α-AgI-like) arrays. Clearly, this hypothesis is consistent with the relative ionic conductivities of the α^* and β phases of Ag_3SI[9] shown in figure 1, since these modifications correspond to 'α-AgI' and 'anti-perovskite' structures, respectively. However, a more detailed comparison of their macroscopic conductivities requires an insight into the relationship between the (static) anion disorder of the bcc sublattice and the (dynamic) cation disorder.

3. The simulation method

The molecular dynamics (MD) simulation technique has been extensively used to probe the diffusion mechanisms within superionic conductors (see [2] and references therein). For the case of Ag_3SI, we adopt the empirical 'RVP' form to describe the interactions between the ions, since this has been used to successfully reproduce the structural properties of both solid and molten Ag_3SI [19, 20] and the transport properties within the binary constituents AgI [21–27] and Ag_2S [28–30]. The general form of the potential between ions i and j described by Rahman, Vashista and Parrinello [21, 22] is

$$V_{ij}(r) = \frac{A_{ij}(R_i + R_j)}{r^7} + \frac{Z_i Z_j e^2}{r} - \frac{1}{2}(\alpha_i Z_j^2 + \alpha_j Z_i^2)\frac{e^2}{r^4} - \frac{W_{ij}}{r^6},$$

where A_{ij} is the short-range repulsive strength, R_i and R_j are the ionic radii, Z_i and Z_j are the ionic charges (which are typically lower than their formal values), α_i and α_j are the electronic polarizabilities and the W_{ij} are the coefficients of the van der Waals interaction. The parameters used in the interionic potentials $V_{ij}(r)$ are summarized in table 1 and their derivation is described below. The values of the coefficients differ somewhat from those used previously to study Ag_3SI [19, 20], principally in the use of different short-range repulsive terms for the S^{2-}–S^{2-}, S^{2-}–I^- and I^-–I^- interactions and the inclusion of van der Waals interactions for the S^{2-}–I^- and I^-–I^- pairs (see table 1).

[9] Using the general notation for the species used in the text, Ag_3SI is a compound of stoichiometry X_3BA.

The values of A_{ij} and W_{ij} for the Ag^+–I^-, Ag^+–S^{2-}, I^-–I^- and S^{2-}–S^{2-} interactions are taken directly from those published previously for AgI [21] and Ag_2S [28, 29]. The A_{AgAg} value is taken as the average of the two slightly different ones given for each binary compound, and A_{SI} and W_{SI} are given as the average of the published values for the corresponding S^{2-}–S^{2-} and I^-–I^- terms [21, 28, 29]. The previously published values for all the R_i are used here, with the exception of R_{Ag}, which is given the average of the values 0.63 Å [21] and 0.61 Å [28, 29] used for AgI and Ag_2S, respectively. The electronic polarizabilities α_i are taken directly from the previous studies [21, 28, 29]. Aside from the implicit assumption of their transferability, the principal difficulty in combining the published potentials for AgI and Ag_2S to give a composite formalism for Ag_3SI lies in the different fractional values of ionic charge used in each case ($Z_{Ag} = +0.60$ and $Z_{Ag} = +0.45$ in AgI [21] and Ag_2S [28, 29], respectively).

To determine the optimum values of Z_{Ag} (and to maintain overall charge neutrality, $Z_I = -Z_{Ag}$ and $Z_S = -2Z_{Ag}$) a number of trial simulations of the binary systems AgI and Ag_2S were performed with differing values of the ionic charge. In the case of bcc structured α-AgI, lowering Z_{Ag} produced a dramatic reduction in the melting temperature of the system, to ∼400 K at $Z_{Ag} = +0.45$. By contrast, increasing Z_{Ag} in the case of bcc structured β-Ag_2S produced relatively minor changes in the simulation, the most significant being a gradual decrease in the Ag^+ diffusion coefficient D_{Ag}. Indeed, the values of D_{Ag} obtained with $Z_{Ag} = +0.60$ are in marginally better agreement with the experimentally determined values [31] than those obtained using the published value of $Z_{Ag} = +0.45$ [28, 29]. We therefore conclude that $Z_{Ag} = +0.60$ represents a good choice for both AgI and Ag_2S and this value is adopted for the case of Ag_3SI in this work.

Simulations were performed at constant (zero) pressure at temperatures over the range 300–900 K using 4 × 4 × 4 cubic unit cells (making a total of 64 × I^-, 64 × S^{2-} and 192 × Ag^+ ions) and were started with the I^- and S^{2-} species ordered over the 0, 0, 0 and $\frac{1}{2}, \frac{1}{2}, \frac{1}{2}$ positions within each unit cell (β-Ag_3SI) or randomly distributed over these sites (α^*-Ag_3SI). A timestep of 0.6 fs was used and all the simulations were allowed to equilibrate for ∼60 ps before a subsequent run of ∼60 ps was performed to analyse the ionic motions. The mean distribution of ions within the unit cell was determined by averaging over time t and over all the unit cells in the simulation box. The diffusion coefficient of the mobile Ag^+, D_{Ag}, was obtained from the slope of the mean-squared displacement at long times, i.e. $D_{Ag} = \lim_{t\to\infty} \frac{1}{6N_{Ag}t} \langle \sum_{j=1}^{N_{Ag}} [r_j(t) - r_j(0)]^2 \rangle$.

4. Results and discussion

The validity of the MD simulations of Ag_3SI will be demonstrated with reference to experimental data for the crystal structures determined by powder neutron diffraction and for the ionic conductivities determined by impedance spectroscopy methods (see [15, 17]). However, a more general analysis of the original neutron diffraction data will be presented here, to provide a description of the time-averaged distribution of the mobile Ag^+ which is not constrained by the imposition of a particular structural model. This procedure uses a maximum entropy difference Fourier analysis, with the positions and (isotropic) thermal vibrations of the S^{2-} and I^- used as the 'known' part of the structure. Details of this technique can be found elsewhere [32]. In addition to providing model-independent descriptions of the ionic distribution, this approach has the advantage over more 'conventional' difference Fourier methods of incorporating prior information, such as the overall positivity of the scattering density distribution and its smoothness on a local scale, in a statistically rigorous manner. Furthermore, analysis of the total scattering from β-Ag_3SI has been carried out using reverse

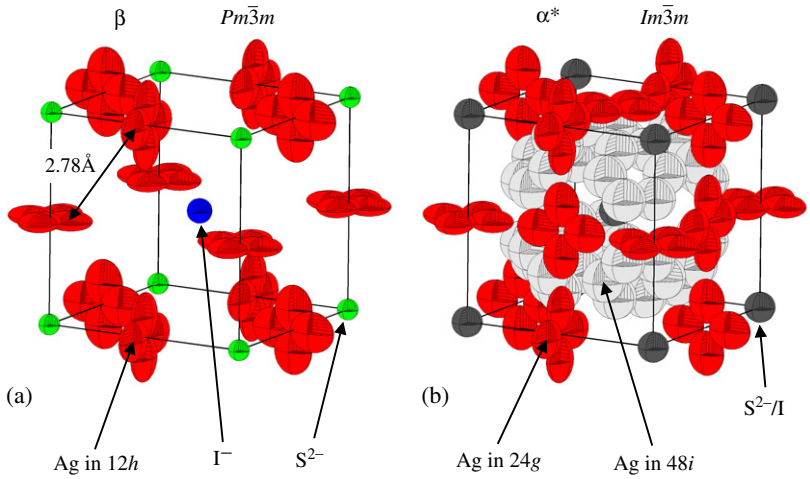

Figure 3. A schematic diagram of the time-averaged structure of (a) β-Ag_3SI at 297(2) K, showing the Ag^+ distribution over the 12*h* sites of space group $Pm\bar{3}m$ and (b) α^*-Ag_3SI at 297(2) K, showing the Ag^+ distribution over the 24*g* and 48*i* sites of space group $Im\bar{3}m$. In the former, the shortest possible distance between pairs of Ag^+ sites (2.78 Å) is illustrated (after [15]).

Monte Carlo (RMC) modelling [33]. The atomistic models produced by this method enable, for example, the extraction of partial radial distribution functions (see section 4.2).

4.1. The β-Ag_3SI phase: time-averaged structure

The crystal structure of the β-Ag_3SI phase determined by least-squares refinement of powder neutron diffraction is illustrated in figure 3(a) [15] and is largely consistent with that predicted by the discussion given in section 2. However, the three Ag^+ are, on average, displaced away from the 'ideal' *oct*1 interstices at $x = 0$ towards the *tet* sites at $x = \frac{1}{4}$ by ≈0.5 Å and are best modelled using partially ($\frac{1}{4}$) occupied 12*h* $x, 0, \frac{1}{2}$ positions of space group $Pm\bar{3}m$, with $x = 0.0986(6)$. The short distances between the 12*h* sites within each group of four (≈0.68 and ≈0.97 Å) dictates that only one of these positions can be occupied at any one time. As a result, the time-averaged structure can alternatively be described as Ag^+ performing anisotropic thermal vibrations about these 12*h* positions or as Ag^+ undergoing extensive and highly anharmonic thermal vibrations about the *oct*1 (3*d*) sites [15]. This ambiguity is demonstrated by the 'model-independent' time-averaged Ag^+ density provided by the maximum entropy difference Fourier analysis of the original neutron diffraction data [15], illustrated in figure 4(a) using a slice taken parallel to the (001) plane between the levels $z = -0.05$ and $+0.05$.

The MD simulations of β-Ag_3SI performed at 300 K indicate that the S^{2-} and I^- undergo predominantly harmonic and isotropic thermal vibrations about their respective positions at the origin and body centre of each unit cell. After averaging over the time span of the simulation and over the $4 \times 4 \times 4$ unit cells, a slice taken parallel to the (001) plane between the levels $z = -0.05$ and $+0.05$ shows that the mean density of Ag^+ determined in the simulation (figure 5(a)) agrees well with that observed experimentally (figure 4(a)). The Ag^+ displacements are highly dynamic (even at ambient temperature) and extend preferentially towards the face centres rather than the body-centre site (i.e. towards the *tet* sites rather than the I^- positions), in accord with the experimental results. The maximum in the Ag^+ density in the simulations is found at $x, 0, \frac{1}{2}$ positions with $x \sim 0.11$, which compares favourably with the experimental value of $x = 0.0986(6)$ [15].

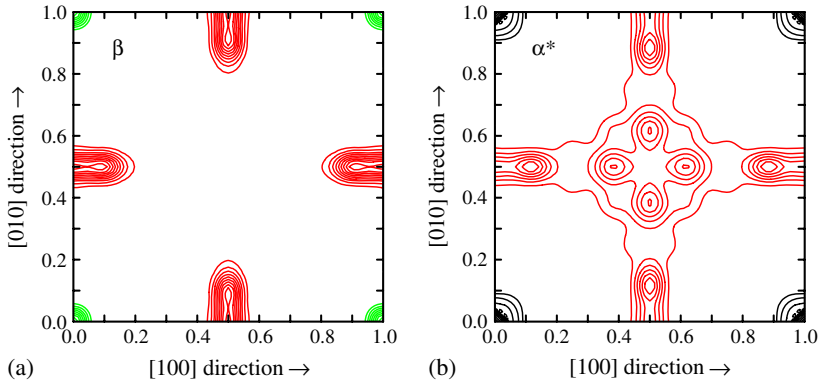

Figure 4. The measured time-averaged density of ions at 297(2) K within a slice taken parallel to the (001) plane between the levels $z = -0.05$ and $+0.05$ for (a) β-Ag_3SI and (b) α^*-Ag_3SI, determined by maximum entropy difference Fourier analysis of powder neutron diffraction data [15].

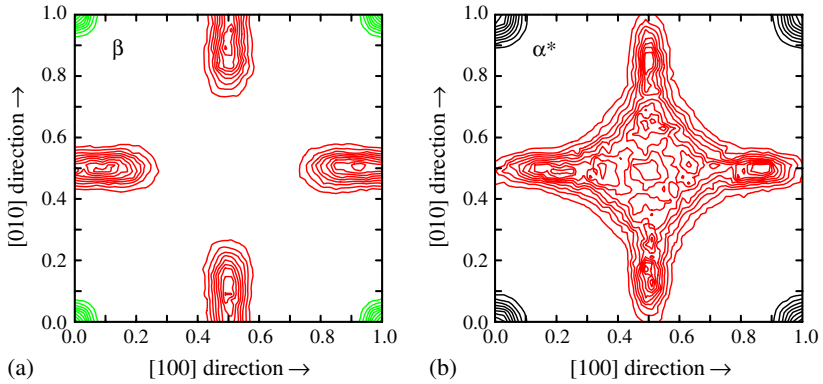

Figure 5. The calculated time-averaged density of ions at 300 K within a slice taken parallel to the (001) plane between the levels $z = -0.05$ and $+0.05$ for (a) β-Ag_3SI and (b) α^*-Ag_3SI, determined by MD simulations using empirical potentials.

4.2. The β-Ag$_3$SI phase: short-range correlations

The good agreement between the simulated and measured *time-averaged* distribution of ions within β-Ag_3SI at ambient temperature is impressive, but does not require that the *instantaneous* correlations between ions are correctly reproduced within the MD calculations. To assess their reliability in this regard, we calculate the partial radial distribution functions, $g_{ij}(r)$, for ion types i and j at each timestep during the simulations, where $g_{ij}(r) = \frac{1}{4\pi r^2\,\mathrm{d}r}\frac{n_{ij}(r)}{\rho_j}$. $n_{ij}(r)$ is the number of ions of type j located at a distance between r and $r + \mathrm{d}r$ from an ion of type i. The number density of ions of type j, ρ_j, is given by $\rho_j = c_j\rho_0$, where ρ_0 is the average number density of ions in the material. It is then possible to generate the total radial distribution function $G(r)$ by summing the individual $g_{ij}(r)$ contributions, weighted by the concentrations of the two species, c_i and c_j, and their neutron scattering lengths, b_i and b_j, so that $G(r) = \sum_{i,j} c_i c_j b_i b_j g_{ij}(r)/(\sum_i c_i b_i)^2$. RMC modelling of total scattering data is also able to probe the instantaneous correlations between ions by refining an atomistic model to scattering data which contain both the Bragg and diffuse components. $10 \times 10 \times 10$ unit cell

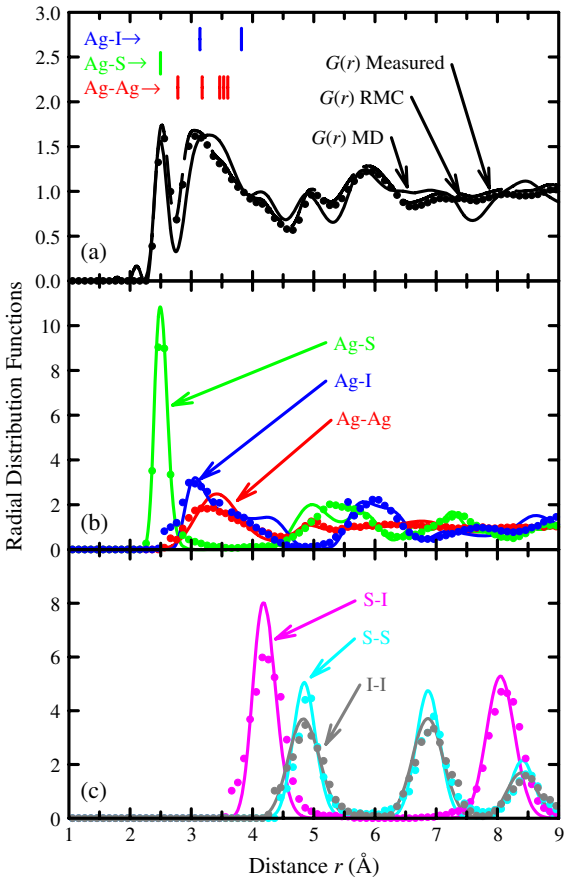

Figure 6. Comparison of (a) the measured total radial distribution function $G(r)$ for β-Ag_3SI (dashed line [15]) with that fitted to the original data using RMC modelling (dots) and that calculated from the MD simulations at 300 K (solid line). The contributions of the three partial radial distribution functions $g_{AgAg}(r)$, $g_{AgS}(r)$, and $g_{AgI}(r)$ are shown in (b) for both MD simulations (solid line) and RMC modelling (dots). The corresponding plot for $g_{SI}(r)$, $g_{SS}(r)$, and $g_{II}(r)$ is shown in (c). The tick marks in (a) indicate the interionic distances calculated for the time-averaged structure of β-Ag_3SI measured at 297(2) K (see figure 3(a) [15]).

supercell models of β-Ag_3SI generated by RMC modelling were in very good agreement with the total scattering structure factor, $F(Q)$, the Bragg intensities and the total radial distribution function, $G(r)$, provided by neutron diffraction measurements [15]. A comparison of the $G(r)$ obtained by Fourier transformation of the experimental $F(Q)$ [15] and those calculated from the MD simulations and RMC models is shown in figure 6. The major features of the experimental $G(r)$ are successfully reproduced by its simulated counterpart, with the most noticeable discrepancy being a displacement of the second peak in the simulated $G(r)$ to higher r values by around 0.2 A. Nevertheless, an important feature observed within all $G(r)$ is the minimum which occurs at ∼2.7 A, since this is close to the shortest possible Ag^+–Ag^+ contact distance of 2.78 A (see figure 3(a)). Inspection of the partial radial distribution functions from the RMC models and MD simulations in figure 6 shows that this minimum occurs between the first peak in $g_{AgS}(r)$ (at 2.51 Å) and a combination of the first peaks in $g_{AgAg}(r)$ and $g_{AgI}(r)$ (at ∼3.0 Å). The lack of density in $g_{AgAg}(r)$ in this region indicates that nearest-neighbour Ag^+

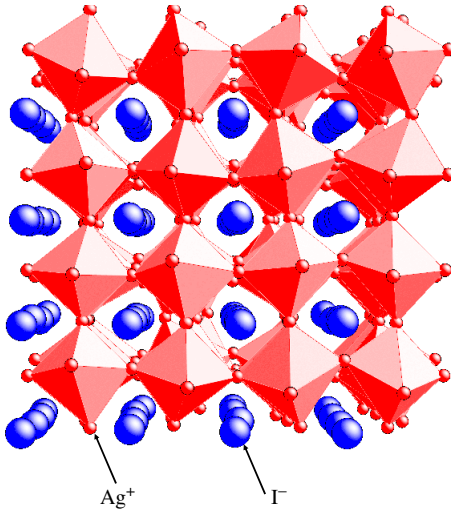

Figure 7. A snapshot of the structure of β-Ag_3SI during the molecular dynamics simulations at 300 K, with the I^- surrounded by eight corner-sharing SAg_6 octahedra. The instantaneous correlations between the locations of neighbouring Ag^+ limit the distortion of the octahedra.

sites are not simultaneously occupied. This means that significant correlations exist between the motions of the nearest-neighbour cations within β-Ag_3SI at temperatures close to ambient. In particular, the displacements of one Ag^+ about its 'ideal' *oct*1 position, which preferentially occur in one of the four $\langle 100 \rangle$ directions perpendicular to the edges of the unit cell, favour displacements of the closest eight Ag^+ which avoid the shortest Ag^+–Ag^+ contacts. As an aside, it is noted that the low-r features in these $g_{ij}(r)$ are markedly different from those published previously [20] where, for example, the lowest-r peak in $g_{AgAg}(r)$ is completely absent. The origin of this discrepancy is unclear, but given that the current MD results agree very well with those from the RMC models the most likely explanation is an error in the $g_{ij}(r)$ calculation in the earlier work.

The instantaneous correlations between the Ag^+ ions in β-Ag_3SI are more easily visualized if we adopt the more commonly used description of the structure of ABX_3 perovskites in terms of a corner-sharing network of BX_6 octahedra. In the case of the 'anti-perovskite' structured β-Ag_3SI, the S^{2-}-centred octahedra are linked by the Ag^+ at their vertices, with each I^- surrounded by eight SAg_6 octahedra. The significant displacements of the Ag^+ away from the *oct*1 positions causes distortions of the idealized corner-sharing array of SAg_6 octahedra, though, as illustrated by the 'snapshot' from the configuration of β-Ag_3SI at 300 K in figure 7, the instantaneous correlations between the Ag^+ limit the extent of the distortions of individual octahedra. Since each SAg_6 octahedron shares each of its vertices with a neighbouring SAg_6 unit, there is instead a tendency towards co-operative tilting of the polyhedral units which extends over several unit cells. However, the SAg_6 units are not completely rigid, and at temperatures close to ambient the correlations between neighbouring Ag^+ persist for typically $\sim$10 ps.

4.3. The β-Ag_3SI phase: Ag^+ diffusion

As the simulation temperature is increased, Ag^+ diffusion is first observed in the β phase at a temperature of 500 K. This process is illustrated in figure 8(a), using the trajectories of the ions within the simulation box shown as a projection down the [001] axis. The amplitude of

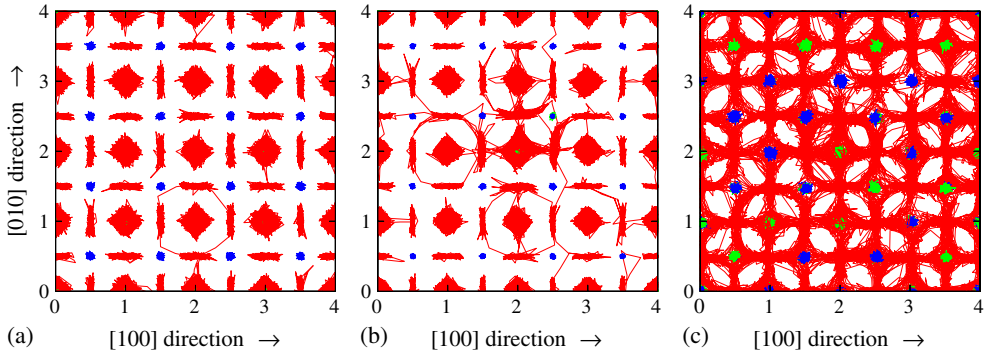

Figure 8. The trajectories of the ions within the 4 × 4 × 4 unit cells within the MD simulations at 500 K, viewed in projection down the [001] direction. In (a) the S^{2-}, and I^- are fully ordered over the 0, 0, 0 and $\frac{1}{2}$, $\frac{1}{2}$, $\frac{1}{2}$ positions, respectively; in (b) a pair of anions at 2.0, 2.0, 2.0 and 2.5, 2.5, 2.5 are swapped and in (c) the S^{2-}, and I^- are randomly distributed.

the vibrations of a single Ag^+ perpendicular to the edge of the unit cell (between two S^{2-}) eventually becomes sufficiently large that a cation can hop in a ⟨110⟩ direction towards the neighbouring Ag^+ site. As discussed in the previous paragraph, significant correlations exist between the dynamic displacements of neighbouring Ag^+ ions, which encourages diffusion of the neighbouring Ag^+. In the example illustrated in figure 8(a), the co-operative diffusion of four Ag^+ correspond to four individual hops perpendicular to the (001) plane (i.e. [110] → $[\bar{1}10]$ → $[\bar{1}\bar{1}0]$ → $[1\bar{1}0]$) and is equivalent to a stepwise 90° rotation of one of the (semi-rigid) SAg_6 octahedra. Simulations at slightly higher temperatures, where Ag^+ diffusion occurs more readily, indicate that ⟨110⟩ hops remain the predominant diffusion mechanism for individual Ag^+, with correlated motion leading to a sequence of such hops. However, only around 60% occur via four coplanar hops of the type illustrated in figure 8(a). Alternative, shorter sequences of hops which form a closed circuit (such as [110] → $[0\bar{1}1]$ → $[\bar{1}0\bar{1}]$) are observed, whilst at temperatures in excess of 700 K a significant fraction of Ag^+ are undergoing ⟨110⟩ hops at a given time and the increasingly dynamic situation makes identification of correlations between the motions of individual Ag^+ impossible.

4.4. The effect of S^{2-}–I^- disorder

To investigate the effect of disorder of the two anion species we use the same simulation box and simulation temperature (500 K) as in the case of β-Ag_3SI shown in figure 8(a), but swap a single pair of nearest-neighbour S^{2-} and I^- (specifically, those at coordinates 2.0, 2.0, 2.0 and 2.5, 2.5, 2.5, respectively). The effect on the simulated trajectories of the Ag^+ is rather dramatic and is illustrated in figure 8(b). The presence of an I^- at the centre of an octahedron of 6 × Ag^+, rather than an S^{2-}, has the effect of expanding the octahedron, since the I^- is the slightly larger anion species. This has the further consequence of enhancing the vibrations of the IAg_6 octahedron and pushing the mean location of the Ag^+ further away from the cube edge. The increased amplitude of the vibrations of the Ag^+ surrounding the I^- enhances their tendency to undergo correlated hops in ⟨110⟩ directions and, since each of the six Ag^+ at the vertices forms an apex of a surrounding SAg_6 octahedron, their Ag^+ are also encouraged to undergo diffusion. As illustrated in figure 8(b), not all of the co-operative Ag^+ diffusion associated with the surrounding SAg_6 octahedra are formed by coplanar sequences of ⟨110⟩ hops, but the Ag^+ diffusion extends over several unit cells in each direction.

4.5. The α^*-Ag_3SI phase: Ag^+ diffusion

The significant increase in the Ag^+ diffusion brought about by the addition of a single S^{2-}–I^- anti-site defect discussed above is remarkable and it provides a clue to the behaviour of the fully disordered α^*-Ag_3SI phase. To investigate the ionic motions in α^*-Ag_3SI, a simulation box was constructed with the S^{2-} and I^- randomly distributed over the *A* and *B* sites. The Ag^+ were initially arranged in an ordered manner over the octahedrally coordinated sites at 0, $\frac{1}{2}$, $\frac{1}{2}$, $\frac{1}{2}$, 0, $\frac{1}{2}$ and $\frac{1}{2}$, $\frac{1}{2}$, 0 (i.e. those sites occupied in fully ordered β-Ag_3SI at temperatures close to ambient), though significant motion of the Ag^+ was observed (even in simulations at 300 K) and the Ag^+ quickly became disordered over all the *oct* sites. For comparison with the simulations of the β phase described above, the trajectories of the ions within α^*-Ag_3SI at a temperature of 500 K are illustrated in figure 8(c). The extensive diffusion of the Ag^+ is clearly visible and, at a first glance, it appears chaotic. However, closer examination of the pattern of cation motion shows that the Ag^+ still predominantly perform hops in ⟨110⟩ directions between sites adjacent to an S^{2-}, in a manner reminiscent of the case of β-Ag_3SI illustrated in figure 8(a).

4.6. The α^*-Ag_3SI phase: time-averaged structure

The time-averaged structure of the α^*-Ag_3SI phase at ambient temperature, determined by powder neutron diffraction methods, is illustrated in figure 3(b) [15]. The S^{2-} and I^- are randomly distributed over the 2*a* sites of space group $Im\bar{3}m$, whilst the Ag^+ are distributed over two different crystallographic sites within the unit cell. Approximately 80% of the cations are located on the 24*g* sites at $x, 0, \frac{1}{2}$ with $x = 0.1301(4)$ and undergo significant anisotropic thermal vibrations. The remaining ≈20% of the Ag^+ are distributed over the 48*i* $\frac{1}{4}, y, \frac{1}{2} - y$ positions with $y = 0.148(3)$. Clearly, this more disordered time-averaged cation distribution is consistent with the higher ionic conductivity of the α^* phase.

The time-averaged density of Ag^+ within α^*-Ag_3SI at 297(2) K, obtained by the maximum entropy difference Fourier analysis of the original neutron diffraction data [15], is shown in figure 4(b). The equivalent cation distribution generated from the MD simulations at 300 K, shown in figure 5(b), is in reasonable agreement with that determined experimentally. However, the simulated Ag^+ distribution appears rather more disordered and bears some resemblance to that obtained from MD simulations of the cation distribution within the superionic phase α-AgI [21, 22].

Comparison of the Ag^+ densities within the β-Ag_3SI and α^*-Ag_3SI phases, using either the experimental or simulated data (figures 4 and 5, respectively), illustrates the correspondence between the 12*h* ($Pm\bar{3}m$) positions occupied by all the cations in the β phase and the 24*g* sites ($Im\bar{3}m$) occupied by the majority of Ag^+ in the α^* form. On these grounds, the structural picture of the α^* phase of Ag_3SI could, to a reasonable approximation, be interpreted as a mixture of two different domains of β-Ag_3SI, corresponding to Ag^+, S^{2-} and I^- located on the *oct*1, *B* and *A* sites, respectively, or on the *oct*2, *A* and *B* sites, respectively (see figure 2(b)). However, for reasonably sized domains (greater than ∼100 Å), this model would be distinguishable from a random distribution of S^{2-} and I^- over the 0, 0, 0 and $\frac{1}{2}$, $\frac{1}{2}$, $\frac{1}{2}$ positions in a Bragg diffraction experiment, owing to the presence of peaks which violate the $h + k + l = 2n$ reflection condition imposed by $Im\bar{3}m$ symmetry.

4.7. Partial ordering of S^{2-} and I^- in Ag_3SI

Whilst data collected by powder neutron diffraction methods from α^*-Ag_3SI are consistent with the space group $Im\bar{3}m$, single-crystal diffraction studies clearly indicate the presence of broad

peaks centred at hkl positions such as 001, 003, 111 and 113, which violate the $h + k + l = 2n$ reflection condition [15]. This observation has been interpreted in terms of ordering of the S^{2-} and I^- species over a short length scale (around ten unit cells), in a manner which resembles their (long-range) ordered arrangement within β-Ag_3SI. Thus, the distribution of the two anion species over the A and B sites in the α^* phase of Ag_3SI samples is not completely random, with the extent of the short-range ordering of S^{2-} and I^- probably dependent on the rate at which the α^* phase is quenched from the high-temperature α phase.

The presence of some degree of short-range order of the two anion species within samples of α^*-Ag_3SI precludes a detailed comparison of the experimental and simulated data for the short-range ion–ion correlations (the total radial distribution function, $G(r)$) because the results of MD simulations were performed with the S^{2-} and I^- distributed completely at random. In principle, configurations of ions containing intermediate levels of short-range order of the S^{2-} and I^- could be constructed and used for MD simulations, but the increased size of the simulation box required to include a reasonable number of localized ordered domains would be computationally prohibitive. Similarly, RMC refinements of this phase would require significantly larger simulation box sizes than those used in this work. Instead, we proceed to consider the difference in Ag^+ diffusion within the simulations of the β and α^* phases, though remaining mindful that the latter represents an idealized case which probably does not occur in real samples of α^*-Ag_3SI because they cannot be quenched from the (fully) disordered α phase sufficiently rapidly.

4.8. Comparison of the α^* and β phases of Ag_3SI

As discussed in section 3, the mean-squared displacement (msd) of the Ag^+ within the MD simulations can be used to estimate the diffusion coefficient, D_{Ag}, However, it is not possible to make a comparison of D_{Ag} for the β and α^* phases of Ag_3SI at ambient temperature because no Ag^+ diffusion occurs in the former (see figure 9(a)). A sufficient level of Ag^+ disorder to allow a reliable estimate of D_{Ag} to be made within the β phase can only be achieved by considering MD simulations performed at 600 K, as shown in figure 9(b). Unfortunately, this is above the temperature of ≈520 K at which (experimentally) the β and α^* phases transform to α-Ag_3SI.

The experimental data for the ionic conductivity of the β and α^* phases shown in figure 1 illustrates that the ratio $\sigma_{\alpha^*}/\sigma_\beta \approx 100$ for $\approx 300\ \text{K} < T < \approx 500\ \text{K}$. Thus, it is reasonable to extrapolate this value to 600 K and make a comparison with the simulated behaviour based on $\sigma_{\alpha^*}/\sigma_\beta$. This has the added advantage of avoiding the calculation of absolute values of ionic conductivity from the simulations using the expression $\sigma = c_{Ag} D_{Ag} Z_{Ag}^2/kT$, where c_{Ag} is the concentration of Ag (i.e. $c_{Ag} = \frac{3}{5}$), which assumes uncorrelated motion of the diffusing species. The presence of significant correlations between the hops of individual Ag^+ in both β and α^* phases of Ag_3SI is highlighted by the simulations presented in sections 4.3–4.5 and are a common feature in many superionic conductors [34]. Furthermore, the above expression contains the ionic charge Z_{Ag}, raising the question whether it is appropriate to use the formal valence of +1.0 or the value $Z_{Ag} = +0.6$ which was employed in the MD simulations (see section 3).

An estimate of $\sigma_{\alpha*}/\sigma_\beta$ for the simulated data at 600 K can be calculated in a straightforward manner using the values of Ag^+ diffusion coefficient, D_{Ag}, obtained from the mean-squared displacements (see figure 9(b)). This gives a value ≈500 which, even allowing for the various assumptions made in its calculation, is significantly higher than the (extrapolated) experimental value of ≈100. Clearly, the greater difference between the ionic conductivities simulated with the anion sublattice completely 'ordered' and 'disordered' is

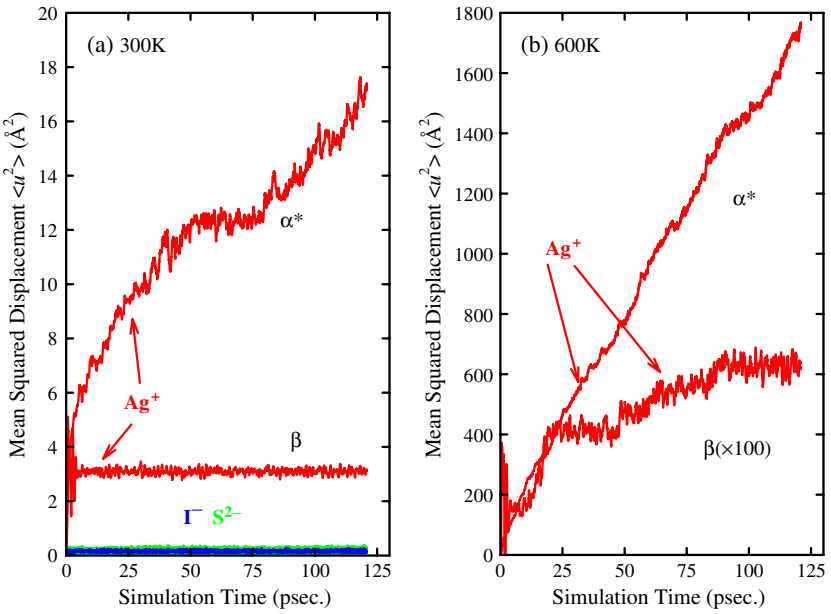

Figure 9. Plots of the mean-squared ionic displacements in β-Ag_3SI and α^*-Ag_3SI at (a) 300 K and (b) 600 K. For clarity, the displacements of the anions are not shown in the latter and the msd data for the β phase have been multiplied by 100.

consistent with a degree of short-range ordering of the S^{2-} and I^- within the sample of α^*-Ag_3SI, as discussed in section 4.7.

5. Discussion and conclusions

The simple crystallographic relationship between the α-AgI ($Im\bar{3}m$) and perovskite ($Pm\bar{3}m$) crystal structures described in section 2 is rarely discussed within the literature, but it has profound implications for the macroscopically observed ionic conductivity. In the case of the anti-perovskite structured compound Ag_3SI discussed here, a disordered arrangement of S^{2-} and I^- over the $0, 0, 0$ and $\frac{1}{2}, \frac{1}{2}, \frac{1}{2}$ sites within the unit cell promotes a significantly higher degree of Ag^+ hops between nearest-neighbour sites in $\langle 110 \rangle$ directions, giving an ionic conductivity over two orders of magnitude higher than the case in which the two anion species are ordered over a long range.

Anti-perovskite structured compounds are rather rare [35], and it is natural to ask whether the same conclusions can be applied to perovskite structured systems in which the (single) anion species is mobile. This question is important for a number of reasons, including suggestions of a superionic phase of $MgSiO_3$ within the earth's lower mantle [36] and potential applications of compounds such as $BaCeO_3$ in solid oxide fuel cells [37]. A clue to the answer is provided by the well-known 'Goldschmidt tolerance factor', which can be written in the form $t_G = (R_A + R_X)/\sqrt{2}(R_B + R_X)$ for a perovskite structured compound of stoichiometry ABX_3 [38]. On geometric grounds, stabilization of the ideal cubic perovskite structure requires $t_G \approx 1$, since this allows both A and B species to adopt coordinations appropriate to their respective sizes (12-fold and 6-fold, respectively).

The transformation from an 'anti-perovskite' to 'perovskite' compound entails swapping the X ions from cations to anions. Since the latter are generally larger than the former, it

follows that the relative size difference between the A and B species must increase in order to meet the Goldschmidt criterion of $t_G \approx 1$. This suggestion is supported by the situation in real compounds, since the anti-perovskite structured Ag_3SI has $R_A/R_B \approx 1.2$ but the perovskite structured $MgSiO_3$ and $BaCeO_3$ have $R_A/R_B \approx 2.2$ and $R_A/R_B \approx 1.9$, respectively [39]. As a consequence, the A and B cation species in a perovskite structured compound are less able to reside within each other's coordination environment. On these grounds, it would be less likely to find a perovskite structure equivalent to Ag_3SI which can be prepared in cation-ordered and cation-disordered polymorphs at ambient temperatures. However, as illustrated by the case of $MPbF_3$ (M = K, Rb and Cs) perovskites, the latter can be stabilized at elevated temperature [40, 41]. The effect of the relative sizes of the two cation species, R_A/R_B, on the ordering of the M^+ and Pb^{2+} species within the bcc sublattice of $MPbF_3$ compounds, and its influence on anion diffusion, will be discussed in a future publication.

Acknowledgments

The work presented in this paper forms part of a wider research project investigating the structural and dynamical behaviour of superionic conductors funded by the Engineering and Physical Sciences Research Council (reference GR/M38711).

References

[1] Chandra S 1981 *Superionic Solids: Principles and Applications* (Amsterdam: North-Holland)
[2] Hull S 2004 *Rep. Prog. Phys.* **67** 1233
[3] Nield V M and Hayes W 1995 *Defect Diffus. Forum* **125/126** 37
[4] Tubandt C and Lorenz E 1914 *Z. Phys. Chem.* **87** 513
[5] Wright A F and Fender B E F 1977 *J. Phys. C: Solid State Phys.* **10** 2261
[6] Nield V M, Keen D A, Hayes W and McGreevy R L 1993 *Solid State Ion.* **66** 247
[7] Boyce J B and Huberman B A 1979 *Phys. Rep.* **51** 189
[8] Boyce J B, Hayes T M and Mikkelsen J C Jr 1981 *Phys. Rev.* B **23** 2876
[9] Miyatani S 1981 *J. Phys. Soc. Japan* **50** 3415
[10] Hull S and Keen D A 2000 *J. Phys.: Condens. Matter* **12** 3751
[11] Hull S and Keen D A 2001 *J. Phys.: Condens. Matter* **13** 5597
[12] Hull S, Keen D A and Berastegui P 2002 *Solid State Ion.* **147** 97
[13] Hull S, Keen D A and Berastegui P 2002 *J. Phys.: Condens. Matter* **14** 13579
[14] Blachnik R and Dreisbach H A 1985 *J. Solid State Chem.* **60** 115
[15] Hull S, Keen D A, Gardner N J G and Hayes W 2001 *J. Phys.: Condens. Matter* **13** 2295
[16] Keen D A and Hull S 2001 *J. Phys.: Condens. Matter* **13** L343
[17] Gardner N J G 1999 Structure and dynamics of superionic conductors at high temperatures and pressures *DPhil. Thesis* University of Oxford
[18] Chiodelli G, Magistris A and Schiraldi A 1979 *Z. Phys. Chem. Neue Folge* **118** 177
[19] Matsunaga S 2003 *J. Phys. Soc. Japan* **72** 1396
[20] Matsunaga S and Madden P A 2004 *J. Phys.: Condens. Matter* **16** 181
[21] Vashishta P and Rahman A 1978 *Phys. Rev. Lett.* **40** 1337
[22] Parrinello M, Rahman A and Vashishta P 1983 *Phys. Rev. Lett.* **50** 1073
[23] Tallon J L 1988 *Phys. Rev.* B **38** 9069
[24] Rains C A, Ray J R and Vashishta P 1991 *Phys. Rev.* B **44** 9228
[25] O'Sullivan K, Chiarotti G and Madden P A 1991 *Phys. Rev.* B **43** 13536
[26] Madden P A, O'Sullivan K F and Chiarotti G 1992 *Phys. Rev.* B **45** 10206
[27] Keen D A, Hull S, Berastegui P, Barnes A C, Crichton W A, Madden P A, Tucker M G and Wilson M 2003 *Phys. Rev.* B **68** 014117
[28] Vashishta P, Ebbsjö I, Dejus R and Sköld K 1985 *J. Phys. C: Solid State Phys.* **18** L291
[29] Ebbsjö I, Vashishta P, Dejus R and Sköld K 1987 *J. Phys. C: Solid State Phys.* **20** L441
[30] Hull S, Keen D A, Sivia D S, Madden P A and Wilson M 2002 *J. Phys.: Condens. Matter* **14** L9
[31] Allen R L and Moore W J 1959 *J. Phys. Chem.* **63** 223

[32] Sivia D S and David W I F 2001 *J. Phys. Chem. Solids* **62** 2119
[33] Tucker M G, Keen D A, Dove M T, Goodwin A L and Hui Q 2007 *J. Phys.: Condens. Matter* **19** 335218
[34] Murch G E 1982 *Solid State Ion.* **7** 177
[35] Mitchell R H 2002 *Perovskites. Modern and Ancient* (Ontario: Almaz Press Inc.)
[36] Matsui M and Price G D 1991 *Nature* **351** 735
[37] Iwahara H 1992 *Solid State Ion.* **52** 99
[38] Goldschmidt V M 1926 *Naturwissenschaften* **14** 477
[39] Shannon R D 1976 *Acta Crystallogr.* A **32** 751
[40] Hull S and Berastegui P 1999 *J. Phys.: Condens. Matter* **11** 5257
[41] Hull S, Berastegui P, Eriksson S-G and Gardner N J G 1998 *J. Phys.: Condens. Matter* **10** 8429